Science Advances

AAAS

advances.sciencemag.org/cgi/content/full/3/4/e1602531/DC1

Supplementary Materials for

Observation of current-induced, long-lived persistent spin polarization in a topological insulator: A rechargeable spin battery

Jifa Tian, Seokmin Hong, Ireneusz Miotkowski, Supriyo Datta, Yong P. Chen

Published 14 April 2017, *Sci. Adv.* **3**, e1602531 (2017)
DOI: 10.1126/sciadv.1602531

This PDF file includes:

note S1. More discussions on the possible mechanisms for the persistent spin polarization, dynamical spin polarization between TSS electrons and nuclear spins, and the interplay of the SML of TSS electrons and hyperfine interaction between the TSS electron spins and nuclear spins.

It is known that transfer of out-of-equilibrium spin polarization between electrons and nuclei can occur through hyperfine interaction (*53*–*57*), allowing dynamic nuclear polarization (DNP) induced by spin-polarized electrons (*58*), for example, the polarized spins injected electrically from a FM (*59*, *60*) or optically (*21*). Conversely, the polarized nuclear spins can induce an electron spin polarization (ESP) and consequently affect the electron transport, which can be used to probe the nuclear spin properties (*42*, *46*, *54*). Recently, the hyperfine interaction between electron spins and the nuclear spins in 3D TIs has been demonstrated or probed in nuclear magnetic resonance (NMR) measurements (*61*–*68*). Figure 7 shows a possible mechanism we propose that may qualitatively explain key features in our observations by considering both the SML and the hyperfine interaction between helically spin-polarized surface state electrons and nuclear spins near the surface in 3D TIs. A large DC bias current I_w can create an out-of-equilibrium helical spin polarization in the conducting electrons in TSS due to the SML, resulting in a large chemical potential difference (*44*) between spin-up and spin-down electrons (eg., Fig. 7, showing the majority "down" spin electrons with higher chemical potential $\mu_\downarrow$ and the minority "up" spin electrons with lower potential $\mu_\uparrow$). An electron from the more occupied "majority" spin state that flips its spin and transfers to the less occupied "minority" spin state will induce an opposite spin flop (eg. from up to down in Fig. 7A) for a nuclear spin near the surface owing to the hyperfine interaction (without which a full spin reversal of a TSS electron would not be allowed by time reversal symmetry) (*45*). Such a hyperfine-interaction-enabled electron-nucleus spin flip-flop process results in a dynamic nuclear spin polarization (NSP) by a current-induced ESP (Fig. 7A). A larger driving current (I_w) gives a larger imbalance in the potential (and population) between majority and minority electron spins, thus more efficient electron-nucleus spin flip-flops and in turn a larger NSP. Reversing I_w reverses the direction of the TSS ESP via SML and also the induced NSP, as shown in Fig.7B. Such a NSP can persist for a long time after the large driving "writing" current (I_w) is removed due to the long lifetime of nuclear spins. Once set up, the NSP could act back on the TSS electron spins again through the hyperfine interaction (through a reverse spin flip-flop) and polarize the electron spins, giving rise to a spin potential difference in electrons (shown in Fig. 7, C and D) that can be measured by spin potentiometry and give an open-circuit spin signal as we observed (Fig. 5). The long time scale (reaching many hours at low temperature, Fig. 5) that the measured spin signal is observed to persist is qualitatively consistent with the long coherence time of the nuclear spins and orders of magnitude longer than the lifetime (typically < 1 μs, in rare cases reaching ~ 1 ms) (*1*, *2*, *5*, *17*, *48*) of electron spin polarization directly injected optically or electrically (*43*). One possible source of nuclear spins with such long life time as observed in our samples (BTS221) may be 77Se, the dominant isotope for Se that has been observed in NMR measurements (*64*, *65*) to have particularly long T1 time (e.g., ~12 h at 60 K, comparable to our observed spin signal persistence time of ~10 h at 45 K), which is much longer compared with 209Bi and 125Te (dominant Bi and Te isotopes), whose T1

are measured to be less than few seconds even at much lower temperatures (*62*, *65–68*). We note that most of these NMR measurements were done in TI samples with more bulk conduction than our bulk-insulating samples, which could have even longer nuclear spin T1 time (due to reduced coupling and relaxation via bulk electrons).

In the presence of a driving current (I_d, which is in fact not needed to detect the persistent electron spin polarization), the electron spin polarization will be determined by the combined effects of the current (I_d) through TSS SML and nuclear spins through hyperfine interaction (the two effects may add or compete with each other depending on their respective preferred spin polarization directions). If I_d is sufficiently weak, the nuclear spins dominate and may effectively "lock" the surface electron spin polarization (ESP) to be unaffected by I_d. This could explain the I_d-independent spin signal we observed. The current (I_w) writing effect in the spin potential signal (which reflects the electron spin polarization) observed in Fig. 2 is a manifestation that the NSP (and in turn the ESP maintained by the nuclear polarization) is set and reversible by the large "writing" current (I_w) as depicted in Fig. 7, A and B. We also note that, in order to observe a notable writing effect, I_w typically needs to be sufficiently large and/or applied for sufficiently long time (Fig. 2 and figs. S5 to S7), consistent with previous reports on current induced NSP in spin-orbit coupled semiconductors (*45*).

On the other hand, if the sample has a much weaker NSP or if the detection current is sufficiently large, the channel spin polarization is mainly determined by the current (I_d) induced ESP via SML of TSS. In this regime, reversing the direction of I_d would reverse the direction of the TSS spin polarization and the measured spin signal, which is expected to increase linearly with increasing I_d, as shown in Ref. *14* and the high current regime in Fig. 3. The transition and qualitatively different behaviors observed in Fig. 3 between the low current ($|I_d|$<~10 μA) regime with largely I_d-independent spin signal (Fig. 3, A and B, dominated by hyperfine interaction) and high current ($|I_d|$>~10 μA) regime with linearly I_d-dependent spin signal (Fig. 3, I and J, dominated by SML) indicate that the effect of NSP induced TSS ESP (via the hyperfine interaction) in this sample becomes comparable with that of current (I_d)-induced TSS ESP (via SML) at a threshold current ~10 μA.

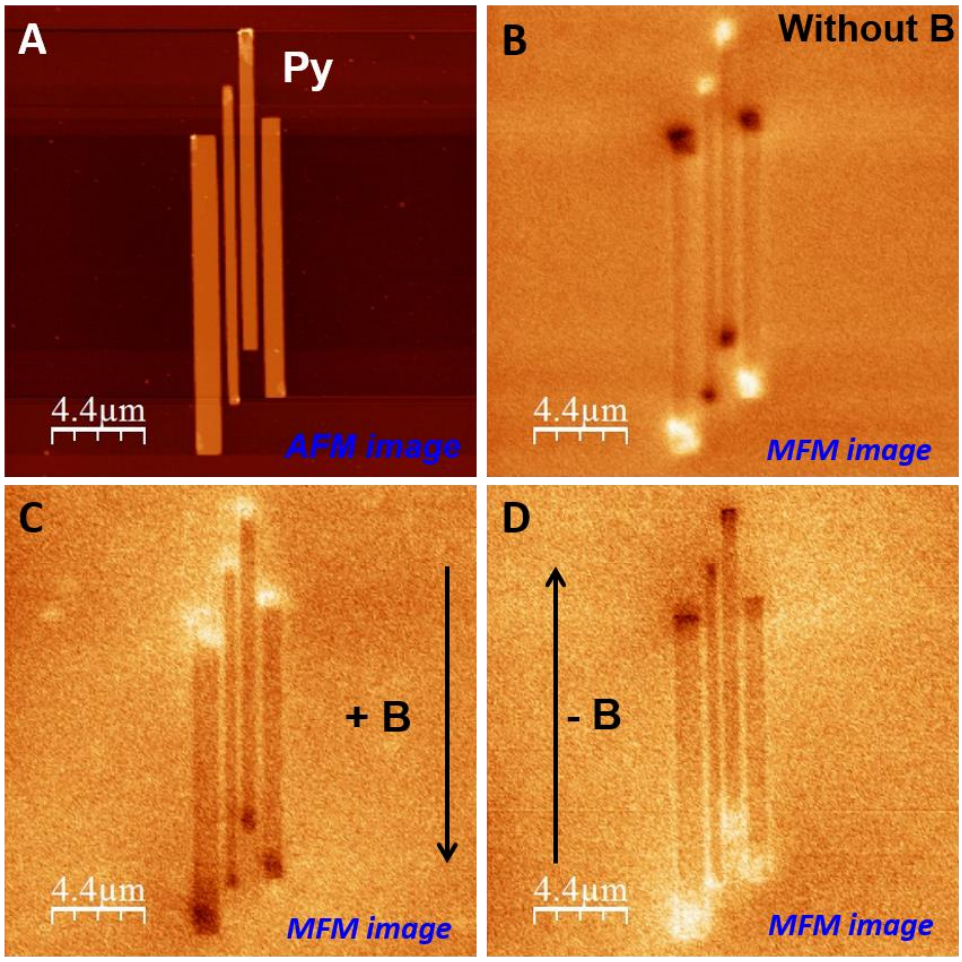

fig. S1. Characterization of the magnetic (Py) electrodes. The atomic force microscope (AFM) and magnetic force microscope (MFM) images of the permalloy (Py) electrodes, measured at room temperature. (**A**) An AFM image of four Py electrodes on SiO_2/Si substrate. The corresponding MFM images of Py (**B**) without applying any magnetic field (*B*) and (**C**) after applying in-plane +*B* field, and (**D**) –*B* field (direction indicated by arrows).

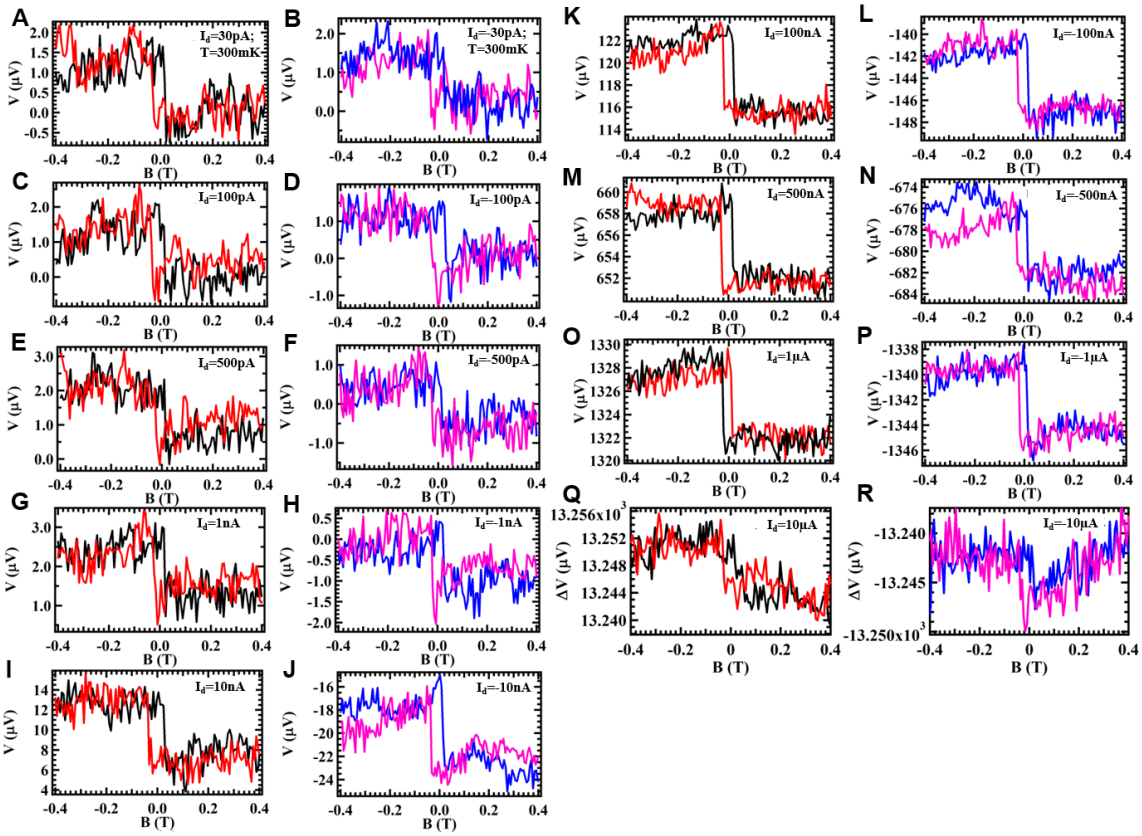

fig. S2. Complete data set on the current dependence of the measured spin signal in device A. (**A** to **R**) The measured voltage as a function of in-plane magnetic field measured on device A at different bias currents of 30 pA (**A**), –30 pA (**B**), 100 pA (**C**), –100pA (**D**), 500 pA (**E**), –500 pA (**F**), 1 nA (**G**), –1 nA (**H**), 10 nA (**I**), –10 nA (**J**), 100 nA (**K**), –100 nA (**L**), 500 nA (**M**), –500 nA (**N**), 1 μA (**O**), –1 μA (**P**), 10 μA (**Q**), and –10 μA (**R**), respectively. All the measurements are performed at T = 300 mK.

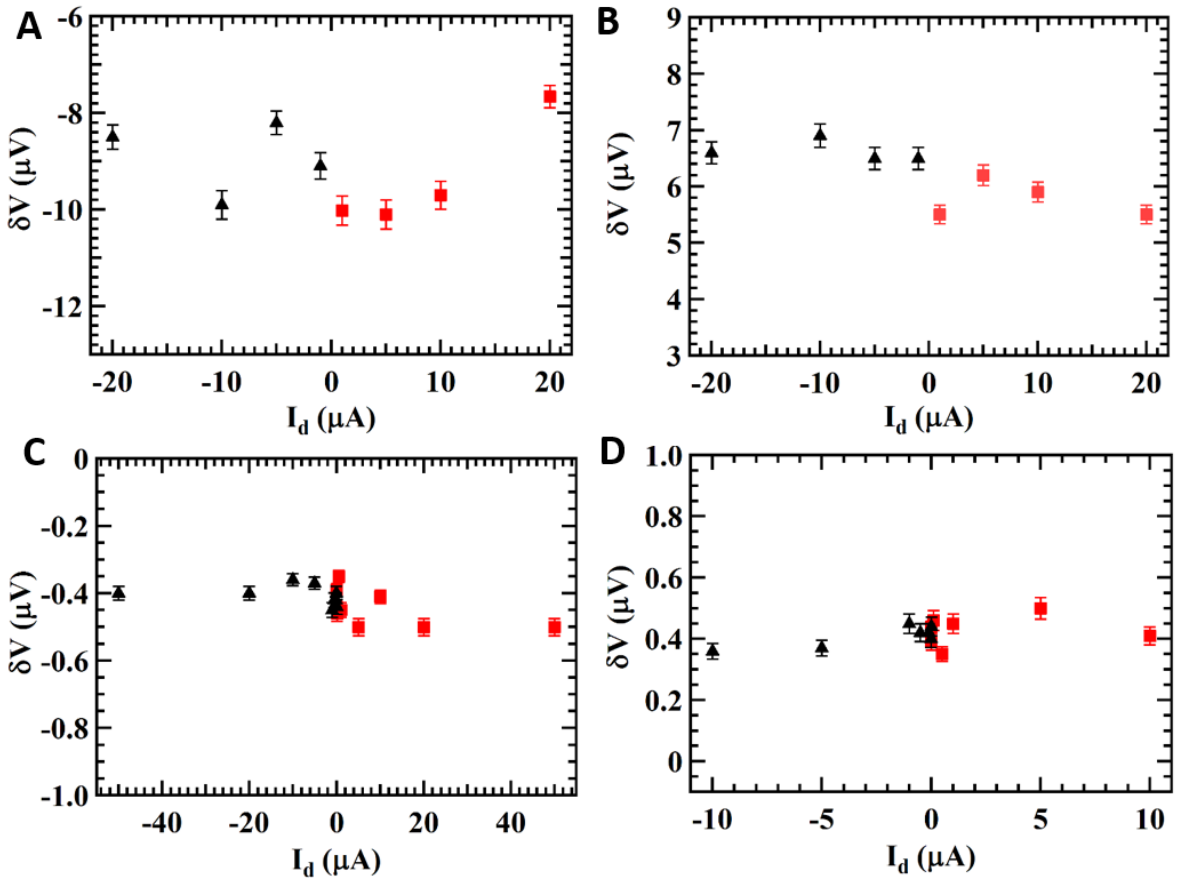

fig. S3. Spin signal largely independent on I_d measured in additional devices. (A to **D)** The spin signal δV as a function of the bias current I_d measured in a few additional BTS221 devices. (A) and (B) Spin signals δV are measured in two different cool-downs of the same device (Device G). (C–D) Spin signals δV are measured on device H and I, respectively. All the measurements are performed at T = 1.6 K.

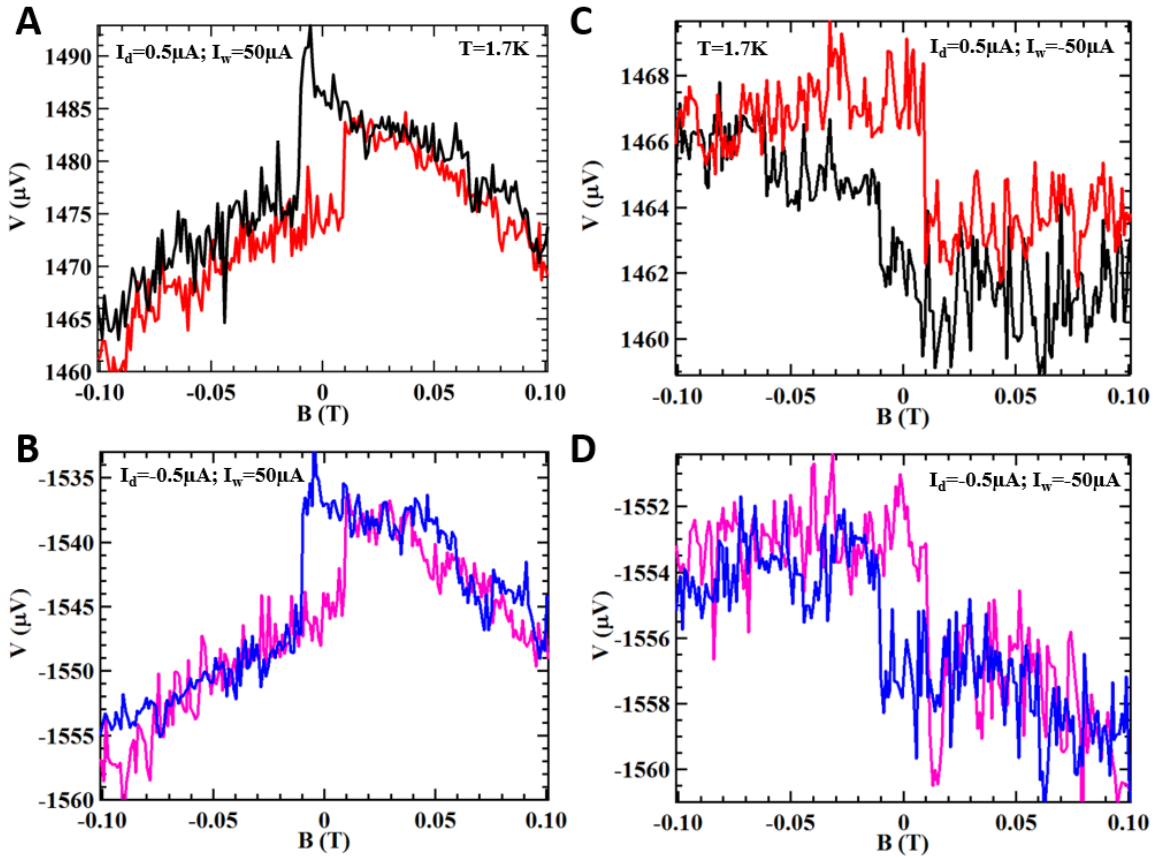

fig. S4. The writing current effect on the spin signal during cooling. Voltage detected by the Py detector as a function of the in-plane magnetic field on device B at small bias currents of 0.5 μA (**A**), –0.5 μA (**B**) after cooling from 76 K to 1.7 K. During the cooling, a large positive "writing" bias current of 50 μA is applied. The Py detector voltage vs in-plane magnetic field measured at small currents of 0.5 μA (**C**), –0.5 μA (**D**) after warming up to 76 K and cooling to 1.7 K again, where a large negative "writing" current of –50 μA is applied during the cooling.

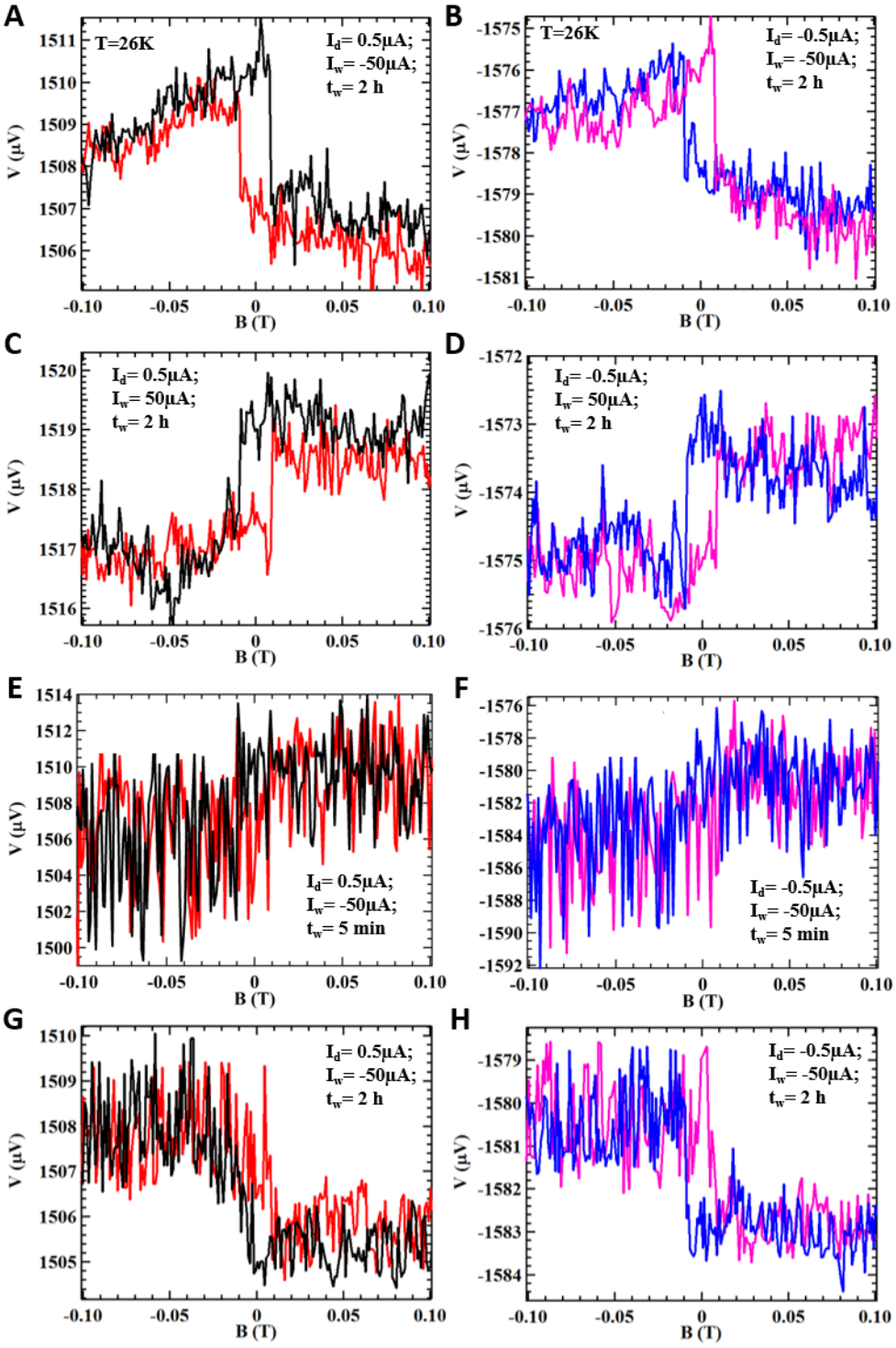

fig. S5. The writing current effect on the spin signal measured at 26 K. (**A** to **F**) Voltage detected by the FM contact as a function of in-plane magnetic field measured on device B at relatively small bias ("detection") currents of 0.5 μA (A, C, E, **G**) and –0.5 μA (B, D, F, **H**) after successively applying a large bias "writing" current (I_w) of –50 or 50 μA for various different duration (t_w). (A and B) I_w = –50 μA for t_w = 2h; (C and D) I_w = +50 μA for t_w = 2h (E and F) –50 μA for 5 min (which is shown to be not long enough to produce notable "writing" effect) (E and F) and –50 μA for 2h (G and H), respectively. All the measurements are performed at 26 K.

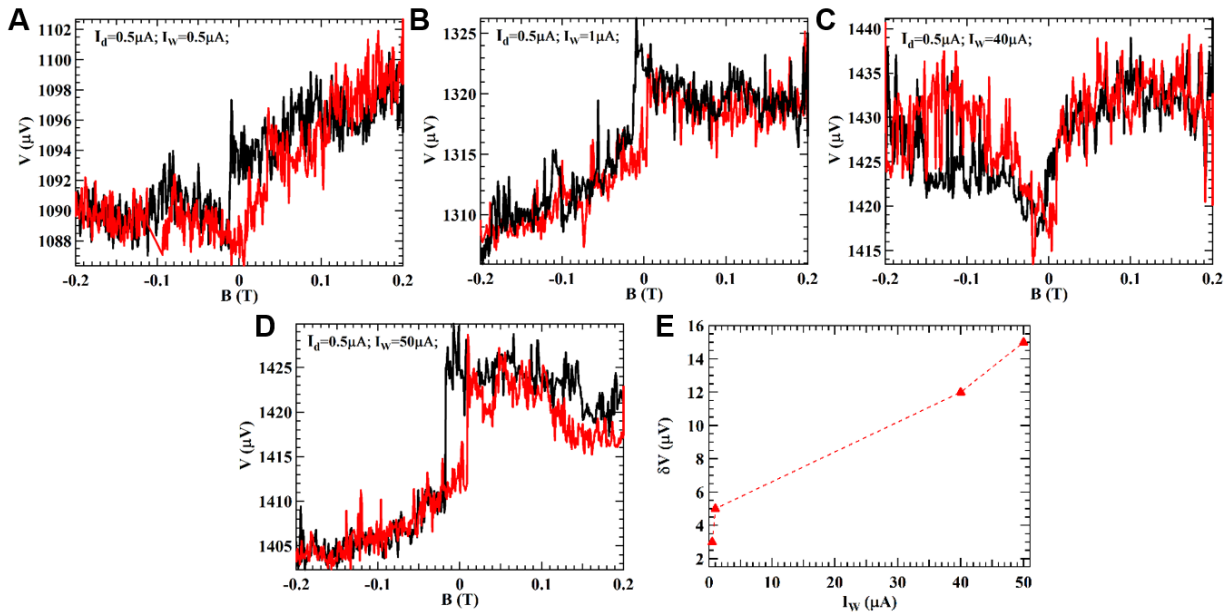

fig. S6. Effect of the magnitude of writing current I_w on the spin signal. Voltage detected by the FM contact as a function of the in-plane magnetic field, measured on device B at a small "detection" current I_d of 0.5 μA after applying a "writing" current I_w of 0.5 μA (**A**), 1 μA (**B**), 40 μA (**C**), and 50 μA (**D**) for 12 h. (**E**) The extracted spin signal δV as a function of the "writing" current I_w. All the measurements are performed at T = 1.6 K. We have found that the observed spin signal is dependent on the writing current (I_w). The "writing" time for each "writing" process is ~12 h, and all the spin signals are measured at a small "detection" current of I_d = 0.5 μA (this small detection current does not affect the observed spin signal, we usually apply such a small detection current with both signs to verify that indeed our spin signal is not dependent on and induced by this small detection current). We can see that the spin signal δV is increasing with the increasing "writing" current I_w, as shown in (E).

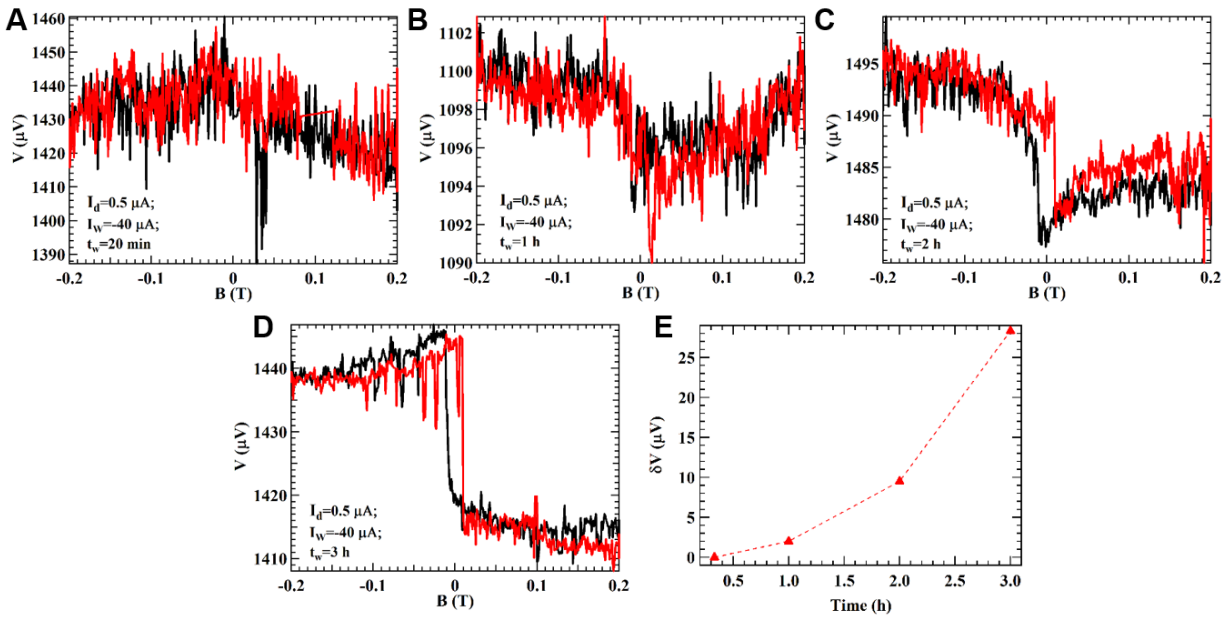

fig. S7. Effect of current writing time on the spin signal. Voltage detected by the FM contact as a function of the in-plane magnetic field, measured on device B at a small "detection" current I_d of 0.5 μA after applying a "writing" current of –40 μA for 20 min (**A**), 1 h (**B**), 2 h (**C**); 3 h (**D**). (**E**) The measured spin signal δV as a function of the "writing" time. All the measurements are performed at T = 1.6 K. We find that the spin signal δV also increases with the "writing" time, as shown in (E). Our results, including the "writing" current (fig. S6) and time (fig. S7)-dependence of the spin signals, further support our "battery" analog (here the writing current is like a charging current for the battery).

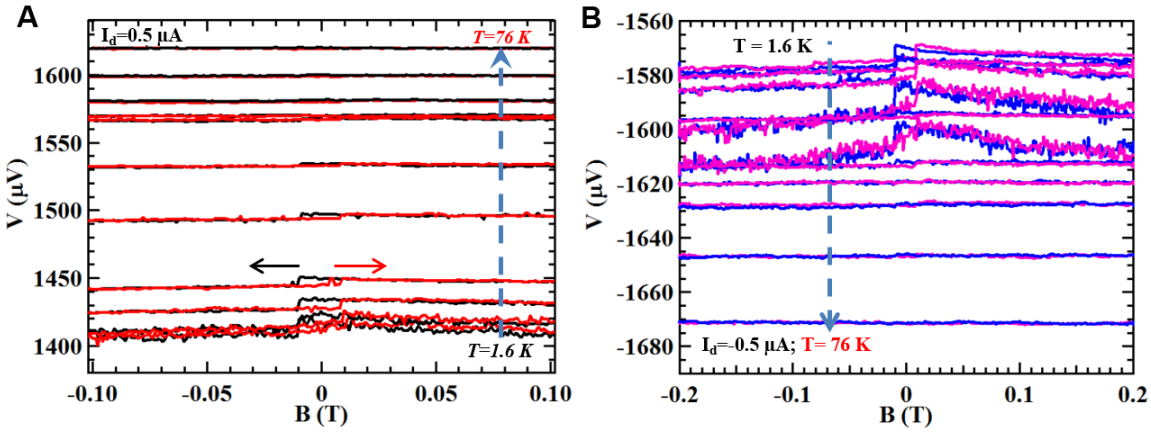

fig. S8. Temperature dependence of the measured spin signal. (**A** and **B**) Voltage measured by the Py spin detector as a function of the in-plane magnetic field measured in device E at a DC bias (detection) current (I_d) of 0.5 μA (**A**) and –0.5 μA (**B**) at various temperatures (T) ranging from 1.6 to 76 K. The red and black arrows indicate the magnetic field sweeping directions.

table S1. Lifetime of the NSP reported in different systems from previous literature. Comparison of our observed long-lived persistent ESP with previously reported typical nuclear spin lifetime.

Materials	Spin lifetime	Temperature	Magnetic field	References
^{31}P-Si	10 h	1.5 K	2 T	Ref. 24
^{31}P-Si	4 ms	125 mK	0 T	Ref. 25
^{28}Si	78 min	300 K	845.3 G	Ref. 26
^{28}Si	120 min	1.9 K	845.3 G	Ref. 26
^{28}Si	22 s	4.2 K	845 G	Ref. 27
^{29}Si	4 h	300 K	174 G	Ref. 28
^{29}Si	4.5 h	300 K	7 T	Ref. 29
Fe/$Al_{0.1}Ga_{0.9}As$/GaAs	600 s	20 K	300 Oe	Ref. 30
GaAs QD	117 s	4 K	2.34 mT	Ref. 31
GaAs QD	1 h	1.7 K	2 T	Ref. 32
InP/$Ga_xIn_{1-x}P$ QD	6000 s	4.2 K	8 T	Ref. 33
InAs QD	40 ms	7 K	0 T	Ref. 34
InGaAs QD	30 h	200 mK	5 T	Ref. 35
InGaAs QD	2.3 s	5 K	0 T	Ref. 36
InGaAs QD	10^5 s	0.2 K	5 T	Ref. 37
(In,Ga)As/GaAs QD	0.3 s	2 K	0 T	Ref. 38
(In,Ga)As/GaAs QD	1 h	6 K	6 T	Ref. 39
GaAs/$Al_xGa_{1-x}As$	600 s	4.2 K	9.1 T	Ref. 40
SiC	8 s	20 K	0 T	Ref. 41
Bi_2Te_2Se (BTS221)	10 h	45 K	< 0.1 T (including 0 T)	This work
Bi_2Te_2Se (BTS221)	> 45 h	1.6 K	< 0.1 T (including 0 T)	This work